ELSEVIER

Journal of Electroanalytical Chemistry 380 (1995) 229–235

JOURNAL OF ELECTROANALYTICAL CHEMISTRY

Structural effects in electron transfer reactions: comparative interfacial electrochemical kinetics for *cis*- versus *trans*-dioxorhenium(V)(bi)pyridine oxidation

Xiao Lian Zhang [a], Joseph T. Hupp [*,a], Gerald D. Danzer [b]

[a] *Department of Chemistry, Northwestern University, Evanston, IL 60093, USA*
[b] *Department of Chemistry, Carthage College, Kenosha, WI, USA*

Received 26 July 1993; in revised form 26 April 1994

Abstract

The comparative interfacial oxidation kinetics of the approximate structural isomers *trans*-$(O)_2Re^V(py)_4^+$ and *cis*-$(O)_2Re^V(bpy)(py)_2^+$ (py, pyridine; bpy, 2,2′-bipyridine) have been assessed in aqueous solution via conventional cyclic voltammetry at a highly ordered pyrolytic graphite (HOPG) electrode. HOPG was employed because of its known propensity to diminish interfacial electron transfer (ET) rates (by ca. three to four orders of magnitude) and because of a probable lack of importance of kinetic work terms (diffuse double-layer corrections). Measured rates for the *trans* complex exceed those for the *cis* by about a factor of 3. Expressed as an effective activation Gibbs energy difference ΔG^*, this corresponds to a *cis–trans* difference of ca. 3 kJ mol^{-1}. The actual vibrational barriers to ET have determined from a combination of published X-ray structural results (*trans* complex) and new resonance Raman results (*cis* complex). The values are 0.6 kJ mol^{-1} for the *trans* oxidation and 4.4 kJ mol^{-1} for the *cis* oxidation (i.e. close to the barrier difference inferred from rate measurements). Further analysis shows that most of the barrier difference is associated with displacement of a (predominantly) Re–N(bpy) stretching mode found only in the *cis* system. Differences in metal-oxo displacements (*cis* > *trans*) are also implicated.

Keywords: Interfacial oxidation kinetics; Structural effects; Electron transfer reactions; Dioxorhenium(V)(bi)pyridine

1. Introduction

We have been exploring the proton-coupled reductions of various dioxorhenium(V) species [1–3] because of the more general insights that they provide into the kinetics and thermodynamics of multielectron transfer processes [4–8]. However, the rhenium(V) complexes are also amenable to proton-decoupled one-electron oxidation – both optically via metal-to-ligand charge transfer excitation [2,3,9–11]

$$trans\text{-}(O)_2Re^V(py)_4^+ \xrightarrow{h\nu} trans\text{-}(O)_2Re^{VI}(py)_3(py^{\bullet -})^+ \quad (1)$$

$$cis\text{-}(O)_2Re^V(bpy)(py)_2^+ \xrightarrow{h\nu} cis\text{-}(O)_2Re^{VI}(bpy^{\bullet -})(py)_2^+ \quad (2)$$

$$cis\text{-}(O)_2Re^V(bpy)(py)_2^+ \xrightarrow{h\nu} cis\text{-}(O)_2Re^{VI}(bpy)(py)(py^{\bullet -})^+ \quad (3)$$

and electrochemically [2,3,9–13]

$$trans\text{-}(O)_2Re^V(py)_4^+ \longrightarrow trans\text{-}(O)_2Re^{VI}(py)_4^{2+} + e^-(\text{electrode}) \quad (4)$$

$$cis\text{-}(O)_2Re^V(bpy)(py)_2^+ \longrightarrow cis\text{-}(O)_2Re^{VI}(bpy)(py)_2^{2+} + e^+(\text{electrode}) \quad (5)$$

where py denotes pyridine and bpy denotes 2,2′-bipyridine.

Our previous studies of electron transfer (ET) thermodynamics [1,2] (see also Brewer and Gray [10]) revealed a strong dependence of the Re(VI/V) formal potential on ligand substituent characteristics (most notably, substituent electron-donating or electron-withdrawing characteristics). The studies also showed, independent of ligand substituent identity, a strong

* Corresponding author.

SSDI 0022-0728(94)03579-R

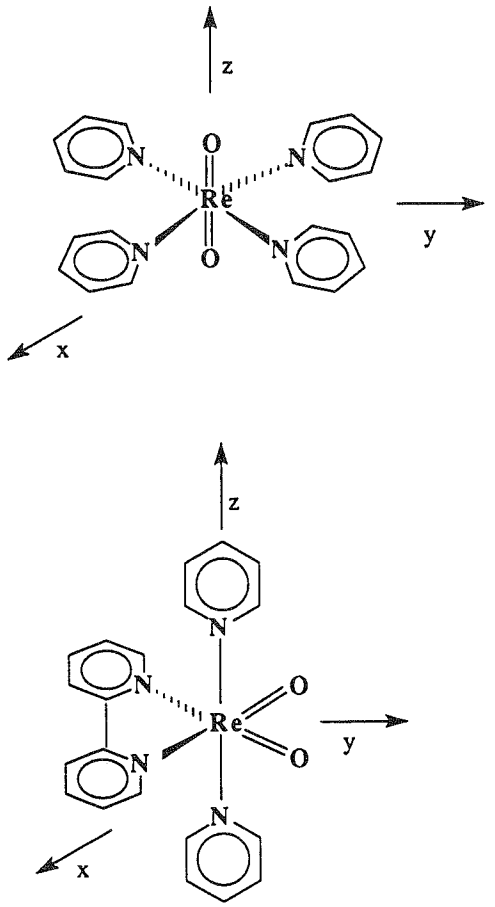

Fig. 1. Chemical structures of *trans*-$(O)_2Re(py)_4^+$ (top) and *cis*-$(O)_2Re(bpy)(py)_2^+$ (bottom).

dependence of E_f on "isomeric" form (i.e. *cis* versus *trans* coordination geometry (Fig. 1)). In all cases the *cis* form was more easily oxidized that the corresponding *trans*, generally by about 600 mV [1].

The origin of the E_f geometry dependence has been explained in terms of the pertinent d-orbital occupancy and the effects of such occupancy upon metal-oxo bonding [3,11,14]. In the *trans* case, the occupied orbital is d_{xy} (where the *z* axis is defined by the dioxorhenium core (Fig. 1)). Removal of one of the two available electrons via Re(V) oxidation should have no effect upon the core—a notion confirmed by crystallographic studies which indicate identical Re–O bond lengths for Re(VI) versus Re(V) [10,15–17]. (Similarly, resonance Raman studies of optical oxidation (Eq. (1)) show that no detectable change in Re–O bond length accompanies the redox transformation [11].) However, for the *cis* form the (doubly) occupied orbital is a composite of d_{xz} and d_{yz}, which unavoidably interacts (unfavorably) with one or more p π^* (oxo) orbitals. Therefore a significant driving force for oxidation ($d^2 \rightarrow d^1$) (Eqs. (2), (3) and (5)) is diminution of the electronic interference and effective enhancement of the Re–O bond order. A corollary is that metal-oxo bond compression should accompany Re(V) oxidation. An X-ray crystal structure for *cis*-$(O)_2Re^{VI}(bpy)(py)_2^{2+}$ has yet to be obtained, and so direct evidence has been lacking. However, resonance Raman studies (reactions (2) and (3)) clearly show that a significant Re–O bond length change accompanies optical oxidation [2,11].

Given the very large thermodynamic and related redox structural differences for *cis*- versus *trans*-dioxorhenium(V) oxidation, we reasoned that large kinetic differences should exist as well [11]. More specifically, because metal-oxo bond length changes accompany the *cis*, but not the *trans*, oxidation, a much higher vibrational activation barrier ought to accompany the *cis* transformation (Eq. (5)). In turn, the rate of the *cis* reaction would be much less than that of the *trans* reaction. Experiments reported here show that an interfacial ET kinetic reactivity difference does exist. Although the difference is smaller than we had initially expected, it is in remarkably good agreement with the predictions of a quantitative multimode Franck–Condon barrier analysis. The analysis is based in part on published crystal structures [10,15–17] and in part on new resonance Raman measurements.

2. Experimental

Dioxorhenium complexes were prepared and purified as previously described [18]. Water was purified by passage through a Milli-Q purification system. Reagent grade sulfuric acid was obtained from the Aldrich Chemical Company Inc. The sodium salt of trifluoromethanesulfonic acid ($NaCF_3SO_3$) was also purchased in reagent grade form from Aldrich. Ungraded (mottled surface) samples of highly ordered pyrolytic graphite (HOPG) were obtained as a gift from Dr. Arthur Moore of Praxair, Parma, OH. Suitable working electrode surfaces were obtained simply by cleaving the HOPG samples via the transparent adhesive tape lift method.

Electrochemical measurements (on HOPG) were made by using a Pine Instruments potentiostat and an "inverted drop cell" geometry (ca. 2–3 mm diameter drop) as described by Kneton and McCreery [19]. The counter-electrode was a platinum wire and the reference was a saturated (NaCl) calomel electrode (SSCE). Reference electrode contact with the drop was achieved via a narrow-tip glass capillary. To minimize double-layer effects as well as *IR* drop effects, fairly concen-

[1] Because of the synthetic inaccessibility of the required *cis*-$(O)_2Re(py)_4^+$ and/or *trans*-$(O)_2Re(bpy)(py)_2^+$ species, true structural isomers could not be compared. Note, however, that the approximate isomers *cis*-$(O)_2Re(bpy)(py)_2^+$ and *trans*-$(O)_2Re(py)_4^+$ differ from each other only by the presence or absence of two aromatic protons and a single inter-ring C–C bond.

trated electrolyte solutions were employed (i.e. 0.1 M H_2SO_4 + 0.5 M $NaCF_3SO_3$). Sample concentrations were typically about 1 mM.

Interfacial ET rates were obtained by comparing digitized experimental cyclic voltammograms with digital simulations generated by the explicit finite-difference method (CVSIM program obtained from Professor D. Gosser, Department of Chemistry, City University, New York [20,21]) or by Nicholson's method [22]. Comparisons were generally made over a range of sweep rates from roughly 20 to 200 mV s^{-1}. (Above 200 mV s^{-1}, distortions evidently due to uncompensated cell resistance were evident.) In view of the relatively high electrolyte concentration and, more importantly, the very low interfacial capacitance (ca. 0.3 $\mu F\ cm^{-2}$ [23]), no diffuse double-layer corrections were employed. However, if corrections had been made, they would have tended to increase both rate constants, with a very slightly larger (relative) increase in the *trans* case (since $E_{pzc} \approx -0.2$ V [23]).

Resonance Raman experiments were carried out essentially as previously described [11]. Prior to analysis, however, the resulting spectra were corrected for both instrument response and sample self-absorption.

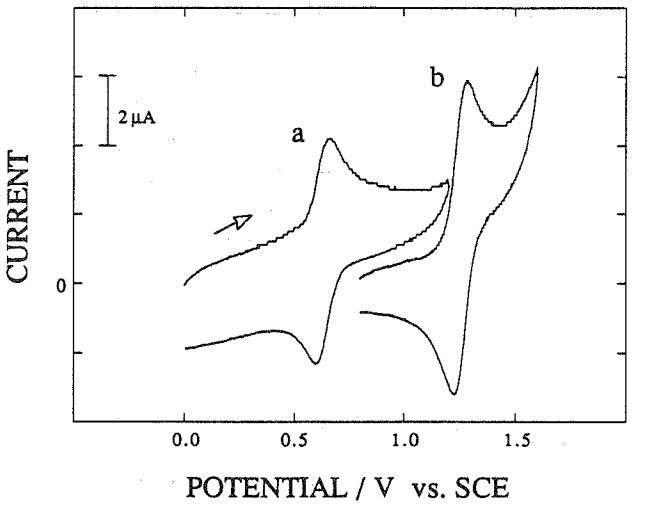

Fig. 2. Cyclic voltammograms (200 mV s^{-1}) at glassy carbon in aq. 0.1 M H_2SO_4 + 0.5 M $NaCF_3SO_3$, for (a) *cis*-$(O)_2Re(bpy)(py)_2^+$ and (b) *trans*-$(O)_2Re(py)_4^+$.

3. Results

3.1. Electrode kinetics

At conventional electrode surfaces such as glassy carbon, both the *cis*- and *trans*-dioxorhenium complexes exhibit purely reversible (i.e. entirely mass transport and redox thermodynamics controlled) voltammetric behavior (see Fig. 2). Therefore this mass transport "masking" makes it impossible to observe ET kinetics differences (at least at conventional cyclic voltammetry sweeping rates). To overcome this difficulty we have turned to HOPG as an electrode material. Kneton and McCreery [19] have shown that HOPG electrodes attenuate interfacial ET rates by ca. three to four orders of magnitude. Although a full explanation of the attenuation effect has yet to be presented, it is almost certainly (in our opinion) an electronic coupling effect arising from the effectively two-dimensional nature of the graphitic material. Consistent with this explanation, McCreery and coworkers [19,23] find that ET rates at HOPG | solution interfaces are strongly dependent on surface defect density (exponentially faster with higher defect density) [19,23]. Importantly, however, they also find [23] that, with carefully handled low-defect-density surfaces, relative rates vary essentially as expected from classical ET activation barrier considerations [24–26].

We have taken advantage of these observations in our evaluation of the molecular geometry dependence of the interfacial ET reactivity of the dioxorhenium-(V/VI) system. Following McCreery and coworkers, we used the kinetics of the model redox system $Fe(CN)_6^{4-/3-}$ as an in-situ probe of defect density [19,23]. He has shown that when the anodic–cathodic voltammetry peak separation ΔE_p for $Fe(CN)_6^{4-/3-}$ exceeds ca. 700 mV, a HOPG surface can be regarded as nearly (but not perfectly!) defect free from an electrode kinetics point of view. Therefore only surfaces which yielded relatively large ΔE_p values (for $Fe(CN)_6^{4-/3-}$) were accepted for subsequent dioxorhenium studies.

In any case, representative voltammograms for *cis*-$(O)_2Re(bpy)(py)_2^{2+/+}$ and *trans*-$(O)_2Re(py)_4^{2+/+}$ at low-defect-density HOPG | aqueous solution interfaces are shown in Fig. 3. Notable observations are (1) that both exhibit comparatively large anodic–cathodic peak separations, clearly indicating interfacial kinetic control of the voltammetry, but (2) that $\Delta E_p(cis)$ exceeds $\Delta E_p(trans)$, implying slower kinetics for the former.

While both findings were qualitatively reproducible, we observed significant experiment-to-experiment variations. To facilitate a more quantitative comparison, we chose to normalize the Re(VI/V) rate constants k_{ET} to those for $Fe(CN)_6^{4-/3-}$ measured immediately before, at the same surface location. (Note that in the "inverted drop cell" geometry, only a fraction of the exposed HOPG surface is in contact with the reactant solution.) The normalization procedure yielded $k_{ET}(cis)/k_{ET}(Fe) = 2.3 \pm 1.0$ and $k_{ET}(trans)/k_{ET}(Fe) = 7.1 \pm 1.8$, where both estimates represent averages of at least five separate experiments and 25 separate rate measurements. In turn, the $k_{ET}(trans)/k_{ET}(cis)$ ratio is estimated as approximately 3.

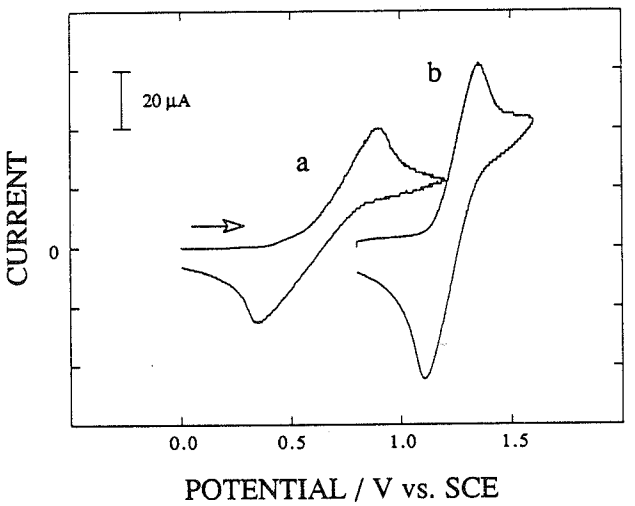

Fig. 3. Cyclic voltammograms (200 mV s^{-1}) at HOPG in aq. 0.1 M H_2SO_4 + 0.5 M $NaCF_3SO_3$, for (a) *cis*-$(O)_2Re(bpy)(py)_2^+$ and (b) *trans*-$(O)_2Re(py)_4^+$. The absolute (unnormalized) ET rate constants in these two particular experiments were k_{ET} (*trans*) = 6.4×10^{-4} cm s^{-1} and k_{ET} (*cis*) = 5.2×10^{-5} cm s^{-1}.

3.2. Structural changes and barrier effects

From standard ET rate theories [24,25] the contribution of internal modes (or vibrations) to the overall reaction barrier (at $E = E_f$) is a simple sum and product function of vibrational frequencies ν and unitless normal coordinate displacements Δ:

$$\Delta G^*_{vib} = (1/8)\sum_i \nu_i \Delta_i^2 \quad (6)$$

where the sum is over all modes which suffer displacement during the reaction. We note that physically Δ is equivalent to four times the number of vibrational levels by which the classical transition state lies above the initially unactivated reactant (for the vibrational mode in question). [2]

Alternatively, for local bonding coordinates, the structure–barrier relationship (again at $E = E_f$) is

$$\Delta G^*_{vib} = (1/8)\sum_j f_j(\Delta a_j)^2 \quad (7)$$

where f is a force constant and Δa is a real bond-length displacement with dimensions of distance. In some instances, specific local modes are sufficiently similar to specific normal modes to permit the following transformation:

$$\Delta a = \left(\Delta^2 h/4\pi\mu\nu b\right)^{1/2} \quad (8)$$

where h is Planck's constant, μ is the reduced mass and b is the "bond degeneracy" (e.g. 2 for Re–O bonds).

[2] The factor of 4 is appropriate when the reactant and product potential energy surfaces are reasonably harmonic and when $\Delta G° = 0$ (i.e. when $E = E_f$).

For *trans*-dioxorhenium(V/VI) we have noted that X-ray structural [15–17] and resonance Raman data [11] indicate (equivalently) that Δa_{Re-O} and Δ_{Re-O} are zero. However, the crystal structures indicate a displacement of the Re–N bonds upon oxidation ($\Delta a_{Re-N} = -0.04$ Å). Transformation via Eqn. (8), with $\mu = 65$, $\nu = 205$ cm^{-1} and $b = 4$, yields $|\Delta_{Re-N}| = 2$. Since no other coordinates are significantly displaced, ΔG^*_{vib} (Eq. (7)) is just 100 cm^{-1} or 1.2 kJ mol^{-1}.

For the *cis* complex, a Re(VI) crystal structure is lacking. Therefore the X-ray approach is not viable for determining coordinate displacements. Nevertheless, the required information can still be extracted via a time-dependent analysis of Raman scattering experiments. The time-dependent theory [27,28] and pertinent applications [29–34] have been discussed in detail elsewhere. However, it may be sufficient to note here that the theory (in its simplest form) leads to the following relationship between enhanced scattering intensities I for any two vibrational modes and the associated frequencies and displacements:

$$I_1/I_2 = \Delta_1^2\nu_1^2/\Delta_2^2\nu_2^2 \quad (9)$$

Importantly, the displacement information obtained is that which is pertinent to the electronic transition giving rise to intensity enhancement. For strongly allowed transitions, Eqn. (9) should be valid at resonance, provided that a reasonably large number of modes is enhanced; at pre-resonance, it should be valid independent of the number of modes enhanced. Note, however, that Eqn. (9) provides only relative coordinate displacements. The required absolute scaling is available from

$$2\sigma^2 = \sum_i \Delta_i^2\nu_i^2 \quad (10)$$

where $8\sigma^2$ is the square of the electronic absorption bandwidth at $1/e$ of the height and where the summation is over all enhanced modes that show significant intensity in the scattering spectrum.

The visible portion of the electronic absorption spectrum for *cis*-$(O)_2Re(bpy)(py)_2^+$ is shown in Fig. 4. Two transitions are evident. The longer-wavelength absorption is due to rhenium-to-bipyridine charge transfer (Eqn. (2)), while the shorter-wavelength absorption is due to rhenium-to-pyridine charge transfer (Eq. (3)). Resonant excitation near 400 nm (see Fig. 4) should lead primarily to enhancement of those Raman scattering modes associated with the latter transition. It is important to note that, from an electrode kinetics point of view, the optical transition (Eq. (3)) is very similar to the interfacial reaction (Eq. (5)). The former transfers an electron to a pyridine π^* orbital that is geometrically orthogonal to (and therefore essentially non-interacting with respect to) the dioxorhenium(VI)-bipyridine plane (see Fig. 1); the latter transfers an

electron to an electrode. In any case, in the scattering experiment we observe enhancement of a number of pyridine-based modes, as well as Re–O and Re–N(bpy) modes. The former obviously gain intensity via displacement effects associated with pyridine radical anion formation (and therefore are irrelevant to our electrochemical investigation). However, the latter are enhanced because of (optical) metal oxidation. Therefore the resulting displacements are identically those of interest in the electrode reaction.

Analysis of scattering intensities via Eqs. 9 and 10 yields $|\Delta_{Re-O}| \approx 0.7$. With $\nu_{Re-O} = 906$ cm^{-1}, $\mu = 15$ g mol^{-1} and $b = 2$, Eqn. (8) yields $\Delta a_{Re-O} \approx \pm 0.04$ Å, where chemical intuition clearly suggests a negative sign for the displacement. In any case, if we view the reaction as one which effectively increases the order of a pair of multiple oxo-metal bonds by ca. 0.25 each, then the estimated extent of the displacement is certainly reasonable [35]. From Eq. (6), the estimated contribution of the dioxometal displacements to ΔG^*_{vib} is 0.6 kJ mol^{-1} (50 cm^{-1}).

The displacement is substantially larger in the Re–N(bpy) mode ($|\Delta| \approx 2.6$) which appears at $\nu = 341$ cm^{-1}. Unlike Re–N(py) and Re–O, this mode is not purely metal–ligand stretching in character (Fig. 5). Consequently, the unitless displacement is not straightforwardly related to any one particular bond length change. Nevertheless, if we assume for the moment that $\nu(341)$ is entirely Re–N(bpy) stretching in character, then an upper-limit estimate for $\Delta a_{Re-N(bpy)}$ can be obtained. On this basis we obtain ± 0.05 Å, where chemical intuition again would strongly suggest bond compression upon oxidation (because electron density is removed from a composite d_{yz}–d_{xz} orbital). Regardless of the details of the local coordinate displacements, however, Eqn. (6) can be used to calculate a barrier contribution of 290 cm^{-1} from $\nu(341)$.

Finally, the Re–N(py) coordinate is also a candidate for displacement. However, resonant scattering from

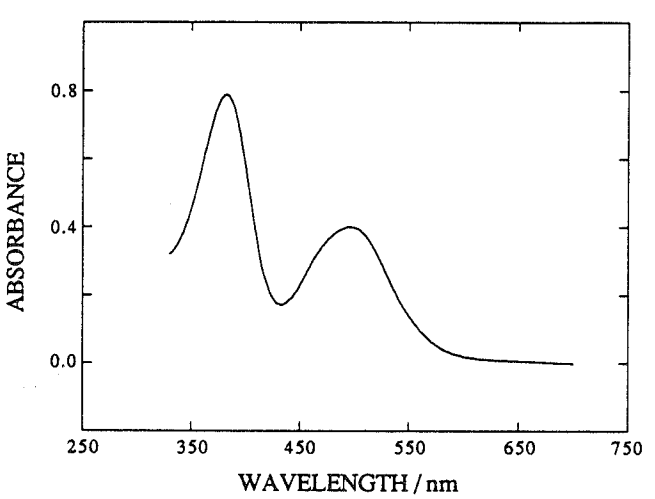

Fig. 4. Electronic absorption spectrum for *cis*-$(O)_2Re(bpy)(py)_2^+$.

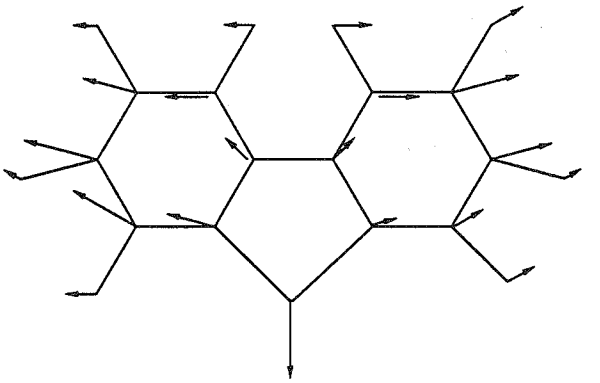

Fig. 5. Normal coordinate motion for $\nu(341)$.

the Re-to-py electronic transition (Eq. (3)) provides an inadequate route to the electrochemically relevant displacement parameter, since obviously the observed $\Delta_{Re-N(py)}$ will also be influenced by $py^{\bullet -}$ formation. A more meaningful estimate can be obtained from resonant scattering from the electronic transition in Eq. (2). Recall that here the electron is transferred to a bpy(π^*) orbital which is geometrically orthogonal to the py–Re–py axis (see Fig. 1). Analysis of Raman data obtained via excitation at 514 nm yields a unitless displacement of ± 1.0. Conversion to local coordinates yields a metal–nitrogen (pyridine) bond length change of ± 0.02 Å, where again the change is very likely negative for Re(V) oxidation. Use of either parameter yields a contribution of 0.3 kJ mol^{-1} (30 cm^{-1}) to $\Delta G^*_{vib}(cis)$. (Re-to-bpy excitation also induces, as expected, a displacement in the Re–O coordinate. Curiously, however, the extent of the displacement is less than half that seen with Re-to-py excitation. For the Re-to-bpy transition an important additional consideration is that the transferred electron generates a radical anion $bpy^{\bullet -}$ which is coordinated to Re(VI) via N atoms which are necessarily *trans* to the oxo ligands (Fig. 1). The resulting "*trans* influence" [36] should act to weaken (and lengthen) both Re–O bonds, thereby offsetting to some extent the strengthening (and shortening) effects anticipated from the rhenium oxidation-state change. This complicating factor would be absent, of course, if the electron were transferred to pyridine instead.)

Summarizing the structural and classical activation barrier effects, we find that (a) $\Delta G^*_{vib}(trans) \approx 0.6$ kJ mol^{-1} (50 cm^{-1}), with contributions from only one vibrational mode, and (b) $\Delta G^*_{vib}(cis) \approx 4.4$ kJ mol^{-1} (370 cm^{-1}), with contributions from three vibrational modes.

4. Discussion

As suggested in Section 1, and reinforced by the structural investigation, significant differences in *cis*

versus *trans* ET reactivity were expected based on significant differences in (classical) Re–O (and Re–N) bond activation requirements. However, the observed rate differences are modest. Some insight can be gained by casting the differences in terms of an effective activation barrier difference. Assuming that

$$k_{ET} = A_{ET} \exp(-\Delta G^*/RT) \quad (11)$$

then

$$\ln k_{ET}(trans) - \ln k_{ET}(cis) = [\Delta G^*(cis) - \Delta G^*(trans)]/RT \quad (12)$$

Based on the kinetic measurements, the effective barrier difference is 3 kJ mol^{-1}, i.e. slightly less than the difference obtained from the structural studies.

One possible mitigating factor in the rate study is that coordinates for high frequency modes will suffer displacement (in part) via tunneling. To the extent that tunneling occurs, the full activation barrier is not surmounted, the apparent barrier to ET is diminished and the ET rate is accelerated. An approximate expression for the tunneling-corrected vibrational barrier is [25,37,38]

$$\Delta G^*_{vib}(\text{corr}) = 0.5RT \sum_i \Delta_i^2 \tanh(h\nu_i/k_B T) \quad (13)$$

where k_B is Boltzmann's constant. For the *trans* reactant (where the barrier consists of a single low frequency displacement) $\Delta G^*_{vib}(\text{corr})$ is essentially identical to the ΔG^*_{vib} value obtained from Eq. (6). For the *cis* complex, $\Delta G^*_{vib}(\text{corr})$ is roughly 0.1 kJ mol^{-1} less than the classical vibrational barrier. This translates into an extremely small rate effect: a calculated 5% enhancement in $k_{ET}(cis)$, virtually all coming from tunneling in the dioxorhenium coordinate.

Finally, a comparison of the one-electron oxidation kinetics with the previously reported two-electron reduction kinetics [1] may be instructive. For the two-electron reactions the geometry dependence is much larger (ca. 100-fold rate difference); furthermore it is reversed (i.e. *trans* is slower than *cis*). For the study described here the relative *trans–cis* kinetics appear primarily to reflect differences in redox-induced structural changes (Franck–Condon effects). In the reduction reactions, related effects may be operative as well. If so, they are clearly overwhelmed by another factor, namely "thermodynamic" access to the intermediate one-electron reduction state. (Expressed another way, the single most important factor is apparently the value of the isolated Re(V/IV) (or Re(IV/III)) potential in comparison with the overall (i.e. Re(V/III)) potential.) Additionally, there are reactivity effects related to the coupling of ET to proton uptake. Of course, these are absent in the pH-independent oxidation processes.

5. Conclusions

HOPG electrodes can be employed to bring the ordinarily quite fast interfacial kinetics of dioxorhenium(V) oxidation into the range of routine experimental accessibility. Within this range, the kinetics of *cis*-dioxorhenium(V) oxidation are consistently slower than those of *trans*-dioxorhenium(V) oxidation. Seemingly consistent with kinetics observations, the *cis* compound suffers a detectable displacement in the symmetric Re–O oxygen stretching coordinate during ET, but the *trans* compound does not. However, a more quantitative analysis shows that differences in metal-oxo displacement are too small, in a Franck–Condon sense, to account for the rate difference. The *cis–trans* reactivity difference instead appears to be related chiefly to differences in Re–N displacements. For the *cis* reaction, these displacements (along with the oxo displacements) can be quantified via a time-dependent analysis of Raman scattering data. The analysis shows that the most important activation barrier component is the symmetrical Re–N(bpy) displacement. However, this component is present only in the *cis* oxidation, thereby accounting for the diminished kinetics for *cis* oxidation compared with *trans* oxidation.

Acknowledgements

We thank the Office of Naval Research for support of this work. JTH also acknowledges support from the Henry and Camille Dreyfus Foundation (Dreyfus Teacher-Scholar Award, 1991–96). We thank Dr. Arthur Moore, Praxair, for providing the HOPG samples and Professor James Kincaid, Marquette University, for providing access to his Raman instrumentation.

References

[1] L.M. Jones-Skeens, X.L. Zhang and J.T. Hupp, Inorg. Chem., 31 (1992) 3879.
[2] M.S. Ram, L.M. Jones, H.J. Ward, Y.-H. Wong, C.S. Johnson, P. Subramanian and J.T. Hupp, Inorg. Chem., 30 (1991) 2928.
[3] M.S. Ram, C.S. Johnson, R.L. Blackbourn and J.T. Hupp, Inorg. Chem., 29 (1990) 238.
[4] T.J. Meyer, J. Electrochem. Soc., 131 (1984) 221c.
[5] H.H. Thorp, J. Chem. Educ., 69 (1992) 250.
[6] M.S. Ram and J.T. Hupp, J. Phys. Chem., 94 (1990) 2378.
[7] D.T. Pierce and W.E. Geiger, J. Am. Chem. Soc., 114 (1992) 6063.
[8] J. Heinze, Angew. Chem. Int. Ed. Engl., 23 (1984) 831.
[9] J.R. Winkler and H.B. Gray, Inorg. Chem., 24 (1985) 346.
[10] J.C. Brewer and H.B. Gray, Reprints: Symp. on Selective Catalytic Oxidation of Hydrocarbons, ACS Division of Petroleum Chemistry, American Chemical Society, Washington, DC, 1990, p 187.

[11] C.S. Johnson, C.S. Mottley, J.T. Hupp and G.I. Danzer, Inorg. Chem., 31 (1992) 5143.
[12] H.H. Thorp, J. Van Houten and H.B. Gray, Inorg. Chem., 28 (1989) 889.
[13] D.W. Pipes and T.J. Meyer, Inorg. Chem., 29 (1986) 3256.
[14] J.C. Dobson, K.J. Takeuchi, D.W. Pipes, D.A. Geselowitz and T.J. Meyer, Inorg. Chem., 25 (1986) 2357.
[15] J.C. Brewer, H.H. Thorp, K.M. Slagle, G.W. Brudvig and H.B. Gray, J. Am. Chem. Soc., 113 (1991) 3171.
[16] C. Calvo, N. Krishnamachari and C.J.L. Lock, J. Cryst. Mol. Struct., 1 (1971) 161.
[17] J.W. Johnson, J.F. Brody, G.B. Ansell and S. Zentz, Inorg. Chem., 23 (1984) 2415.
[18] M.S. Ram and J.T. Hupp, Inorg. Chem., 30 (1991) 130.
[19] K.R. Kneton and R.L. McCreery, Anal. Chem., 64 (1992) 2518.
[20] D.K. Gosser and F. Zhang, Talanta, 38 (1991) 715.
[21] Q. Huang and D.K. Gosser, Talanta, 39 (1992) 1155.
[22] R.S. Nicholson, Anal. Chem., 37 (1965) 1355.
[23] M.T. McDermott, K. Kneton and R.L. McCreery, J. Phys. Chem., 96 (1992) 3124.
[24] N. Sutin, Prog. Inorg. Chem., 30 (1983) 441.
[25] N. Sutin, Comments Inorg. Chem., 6 (1987) 209.
[26] M.J. Weaver in R.G. Compton (Ed.), Comprehensive Chemical Kinetics, Vol. 27, Elsevier, Amsterdam, 1988.
[27] E.J. Heller, Acc. Chem. Res., 14 (1981) 368.
[28] E.J. Heller, R.L. Sundberg and D. Tannor, J. Phys. Chem., 86 (1982) 1822.
[29] J.I. Zink and K.-S.K. Shin in D.H. Volman, G.S. Hammond and D.C. Neckers (eds.), Advances in Photochemistry, Vol. 16, Wiley, New York, 1991, p. 119.
[30] S.K. Doorn, R.L. Blackbourn, C.S. Johnson, and J.T. Hupp, Electrochim. Acta, 36 (1991) 1775.
[31] R.L. Blackbourn, S.K. Doorn, J.A. Roberts and J.T. Hupp, Langmuir, 5 (1989) 696.
[32] S.K. Doorn and J.T. Hupp, J. Am. Chem. Soc., 111 (1989) 4704.
[33] R.L. Blackbourn, C.S. Johnson and J.T. Hupp, J. Am. Chem. Soc., 113 (1991) 1060.
[34] F. Markel, N.S. Ferris, I.R. Gould and A.B. Myers, J. Am. Chem. Soc., 114 (1992) 6208.
[35] W.A. Nugent and J.M. Mayer, Metal–Ligand Multiple Bond, Wiley, New York, 1988.
[36] F.A. Cotton and G. Wilkinson, Advanced Inorganic Chemistry (5th ed.), Interscience, New York, 1988, p. 300.
[37] B.S. Brunschwig, J. Logan, M.D. Newton and N. Sutin, J. Am. Chem. Soc., 102 (1980) 5798.
[38] T. Holstein, Philos. Mag., 37 (1978) 49.